DIGITAL SYNTHESIS MODELS OF CLARINET-LIKE INSTRUMENTS INCLUDING NONLINEAR LOSSES IN THE RESONATOR

Philippe Guillemain, Jonathan Terroir

CNRS – Laboratoire de Mécanique et d'Acoustique
31 ch. J. Aiguier, 13402 Marseille cedex 20, France
{guillem|terroir}@lma.cnrs-mrs.fr

ABSTRACT

This paper presents a real-time algorithm for the synthesis of reed instruments, taking into account nonlinear losses at the first open tonehole. The physical model on which the synthesis model relies on is based on the experimental works of Dalmont et al. who have shown that for high pressure levels within the bore, an air jet obeying the Bernoulli flow model, hence acting as a nonlinear resistance, is created at the open end of the bore. We study the effect of these additional losses on the response of the bore to an acoustic flow impulse at different levels and on the self oscillations. We show that at low frequencies, these nonlinear losses are of the same order of magnitude than the viscothermal linear losses and modifie the functioning of the whole instrument. For real-time synthesis purposes, a simplified algorithm is proposed and compared to the more accurate model.

1. INTRODUCTION

Many works have been devoted to the physical study and the modeling of toneholes in woodwind instruments (see *e.g.* [1] and [2]) and digital resonator models including toneholes (see *e.g.* [3] and [4]) have been proposed for the real-time simulation of these instruments. These synthesis models describe toneholes, or more generally the "open termination" of an instrument as a passive linear element of the resonator which can then be fully characterized by its input impedance or by the linear relationship between the wave variables. Experimental studies [5] have shown that for high levels of acoustic pressure and flow within the bore of the instrument, nonlinear effects may appear, mainly due to the formation of a dissipative air jet at the open end, comparable to the one responsible of the birth of self oscillations at the mouthpiece level. While impedance measurements are done at low acoustic pressure and flow levels, pressure levels within the bore are very high under normal playing conditions and the nonlinear behavior of the termination can probably no longer be ignored.

In this paper, in order to quantify the relative weight of these nonlinear additional losses with respect to the classical, linear, viscothermal losses, we propose a real-time oriented synthesis model of clarinet-like instruments taking into account a nonlinear termination. The physical model is based on the experimental works of Dalmont [5] and the synthesis model is a modified version of the model presented in [6].

The paper is organized as follows. The physical model of a nonlinear dissipative termination is first presented. A time domain digital model, and a simplified version are then proposed. It is then shown that the nonlinear termination has a significant role on the response of the bore. Finally, the self oscillations of a full instrument model are studied and comparison is made between the classical linear model and the two nonlinear models proposed, showing that a very simple algorithm is able to reproduce the behaviors observed on a more complicated one. The nonlinear termination is shown to modify significantly the functioning and the timbre of the instrument.

2. BORE MODEL

The physical model on which is based the synthesis model is first summarized. Two digital formulations are presented and the effect of the nonlinear termination on the bore response is studied on the most accurate one.

2.1. Physical model

A perfectly cylindrical resonator is considered. One assumes linear propagation within the bore.

The wavenumber is denoted $k(\omega)$ and includes propagation delay, dispersion and dissipation corresponding to viscothermal effects. It is classically given by [7] :

$$k(\omega) = \frac{\omega}{c} - \frac{j^{3/2}}{2}\eta c\omega^{1/2}$$

$Z_c = \frac{\rho c}{S}$ is the characteristic impedance of the bore, $S = \pi R^2$ is the input surface of the bore and η is given by:

$$\eta = \frac{2}{Rc^{3/2}}\left(\sqrt{l_v} + \left(\frac{c_p}{c_v} - 1\right)\sqrt{l_t}\right)$$

R is the radius of the bore: $R = 7.10^{-3}$ in the clarinet case. Typical values of the physical constants, in mKs units, are: $c = 340$, $l_v = 4.10^{-8}$, $l_t = 5.6.10^{-8}$, $C_p/C_v = 1.4$.

2.1.1. Linear bore model

If the radiation impedance at the open end is taken into account only as a length correction, the acoustic pressure $p_s(t)$ at the end of the bore vanishes, and the input impedance of the bore, which is the ratio between the Fourier transforms (denoted with capital letters) of the acoustic pressure $p_e(t)$ and acoustic flow $u_e(t)$ at the mouthpiece level is classically expressed by:

$$\frac{P_e(\omega)}{U_e(\omega)} = jZ_c \tan(k(\omega)L) \qquad (1)$$

where L is the total length of the bore, including the length correction corresponding to the radiation impedance.

2.1.2. Nonlinear bore model

When nonlinear losses at the open end are considered, the input impedance is not well defined. Indeed, according to Dalmont [5], the nonlinear termination of the open end of the bore is defined in the time domain by:

$$\frac{p_s(t)}{u_s(t)} = (0.6 \pm 0.1)\frac{|v_s(t)|}{c}Z_{ct} \quad (2)$$

where $v_s(t)$ is the mean acoustic velocity, averaged on the radiating surface S_t and $Z_{ct} = \rho c/S_t$ is the characteristic impedance corresponding to the radius r_t of the open end. The coefficient (0.6 ± 0.1) has been determined experimentally.

It is worth noting that equation (2) corresponds to a classical Bernoulli flow model since it can be rewritten as $p_s(t) = \frac{1}{2}\rho v_s^2(t)$ by considering the $(-)$ sign in (0.6 ± 0.1) and assuming that after the dissipation of the jet created by the hole, the pressure outside the resonator is zero. Hence, for the sake of simplicity and for synthesis purposes, we shall assume that the surface S_t at the open end corresponds to the surface of the first open tonehole and can be smaller than the surface S of the resonator. Such an approximation, which considers that the equivalent length of a resonator corresponds to the distance between the mouthpiece and the first open tonehole and ignore the resonator characteristics after the first open tonehole seems relevant in the context of this study.

From equation (2), one obtains in terms of pressure and flow variables:

$$p_s(t) = \alpha \,|u_s(t)|\, u_s(t) \quad (3)$$

where $\alpha = \dfrac{0.6Z_{ct}}{cS_t}$. Equation (3) shows that the open end acts as a nonlinear resistance which is proportional to the absolute value of the acoustic flow.

In order to take into account these nonlinear losses in the bore model, we consider the classical transmission line equations between the input and the output of the bore:

$$\begin{cases} P_e - Z_cU_e = e^{-jk(\omega)L}(P_s - Z_cU_s) \\ P_s + Z_cU_s = e^{-jk(\omega)L}(P_e + Z_cU_e) \end{cases} \quad (4)$$

2.2. Digital model

In order to propose a time domain digital formulation of the system of equations (4), the propagation described by $e^{-jk(\omega)L}$ is first approximated by:

$$e^{-jk(\omega)L} \approx \frac{\beta_0}{1 - \alpha_1 z^{-1}}z^{-D} \quad (5)$$

where $z = e^{\frac{j\omega}{F_e}}$, F_e is the sampling frequency and $D = E\left(\frac{F_eL}{c}\right)$. The coefficients β_0 and α_1 are calculated according to [6] and correspond to the propagation over a length L.

In order to be able to collect versions of p_s and u_s delayed by D, that are required for the computation of p_e with the first equation of system (4), the second equation of system (4) is written as:

$$(P_s + Z_cU_s)e^{-jk(\omega)L} = e^{-2jk(\omega)L}(P_e + Z_cU_e) \quad (6)$$

which yields:

$$\frac{\beta_0}{1 - \alpha_1 z^{-1}}z^{-D}(P_s + Z_cU_s) = \left(\frac{\beta_0}{1 - \alpha_1 z^{-1}}z^{-D}\right)^2(P_e + Z_cU_e) \quad (7)$$

thus:

$$(P_s + Z_cU_s)(1 - \alpha_1 z^{-1})z^{-D} = \beta_0(P_e + Z_cU_e)z^{-2D} \quad (8)$$

Using the same approximation of propagation and losses, the first equation of system (4) becomes:

$$P_e - Z_cU_e = \frac{\beta_0}{1 - \alpha_1 z^{-1}}z^{-D}(P_s - Z_cU_s) \quad (9)$$

yielding:

$$(P_e - Z_cU_e)(1 - \alpha_1 z^{-1}) = \beta_0(P_s - Z_cU_s)z^{-D} \quad (10)$$

In the time domain, the digital equivalent of system (4) becomes:

$$\begin{cases} p_s(n-D) + Z_cu_s(n-D) = \alpha_1[p_s(n-D-1) \\ \quad + Z_cu_s(n-D-1)] + \beta_0[p_e(n-2D) + Z_cu_e(n-2D)] \\ p_e(n) = Z_cu_e(n) + \alpha_1[p_e(n-1) - Z_cu_e(n-1)] \\ \quad + \beta_0[p_s(n-D) - Z_cu_s(n-D)] \end{cases} \quad (11)$$

In order to integrate this resonator model in a full instrument model including a reed and a nonlinear coupling at the entrance of the resonator, we use the dimensionless variables defined by [8]: $\tilde{p}_{e,s} = \dfrac{p_{e,s}}{p_M}$ and $\tilde{u}_{e,s} = Z_c\dfrac{u_{e,s}}{p_M}$ where p_M is the static beating-reed pressure.

This change of variables leads to:

$$\begin{cases} \tilde{p}_s(n-D) + \tilde{u}_s(n-D) = \alpha_1[\tilde{p}_s(n-D-1) \\ \quad + \tilde{u}_s(n-D-1)] + \beta_0[\tilde{p}_e(n-2D) + \tilde{u}_e(n-2D)] \\ \tilde{p}_e(n) = \tilde{u}_e(n) + \alpha_1[\tilde{p}_e(n-1) - \tilde{u}_e(n-1)] \\ \quad + \beta_0[\tilde{p}_s(n-D) - \tilde{u}_s(n-D)] \end{cases} \quad (12)$$

In the same way, a dimensionless coefficient corresponding to the nonlinear losses α is defined: $\tilde{\alpha} = \dfrac{(0.6 \pm 0.1)p_M}{\rho c2}\dfrac{S^2}{S_t^2}$.

With this change of variables, the instantaneous nonlinearity at the open end of the bore corresponding to equation (3) becomes:

$$\tilde{p}_s(n-D) = \tilde{\alpha}\,\text{sign}(\tilde{u}_s(n-D))\tilde{u}_s(n-D)^2 \quad (13)$$

From the first equation of system (12) and equation (13), the value of $\tilde{u}_s(n-D)$ can be obtained analytically by solving the equation:

$$\tilde{\alpha}\,\text{sign}(\tilde{u}_s(n-D))\tilde{u}_s^2(n-D) + \tilde{u}_s(n-D) - \tilde{V}_s = 0 \quad (14)$$

where:

$$\tilde{V}_s = \alpha_1(\tilde{p}_s(n-D-1) + \tilde{u}_s(n-D-1)) \\ + \beta_0((\tilde{p}_e(n-2D) + \tilde{u}_e(n-2D)) \quad (15)$$

By considering successively the cases $\tilde{u}_s(n-D) \geq 0$ and $\tilde{u}_s(n-D) < 0$, since $\text{sign}(\tilde{u}_s(n-D)) = \text{sign}(\tilde{p}_s(n-D)) = \text{sign}(\tilde{V}_s)$, $\tilde{u}_s(n-D)$ is finally given by:

$$\tilde{u}_s(n-D) = \text{sign}(\tilde{V}_s)\frac{-1 + \sqrt{1 + 4\,\text{sign}(\tilde{V}_s)\tilde{\alpha}\tilde{V}_s}}{2\tilde{\alpha}} \quad (16)$$

At any time sample n, the process leading to the calculation of the output $\tilde{p}_e(n)$ from any arbitrary input $\tilde{u}_e(n)$ consists in the sequential calculation of:

- $\tilde{V}_s$ with equation (15)
- $\tilde{u}_s(n - D)$ with equation (16)
- $\tilde{p}_s(n - D)$ with equation (13)
- $\tilde{p}_e(n)$ with the second equation of system (12)

It is worth noting that the case of a linear termination corresponds to assume that $\forall n, \tilde{p}_s(n) = 0$ and $\tilde{u}_s(n - D) = \tilde{V}_s$

2.3. Simplified digital model

For the sake of simplicity and computational efficiency, we seek a digital resonator model that uses as few physical variables as possible and requires as less computation power as possible, while keeping the most important features of a more sophisticated model. As a first simplification, we seek an approximation that allows to remove the variables $\tilde{p}_s$ and $\tilde{u}_s$ of the whole scheme.

For that purpose, equations (7) and (9) modelling propagation in both directions are written in the following way:

$$
\begin{cases}
\frac{\beta_0}{1 - \alpha_1 z^{-1}} z^{-D}(P_s + Z_c U_s) = \frac{b_0}{1 - a_1 z^{-1}} z^{-2D}(P_e + Z_c U_e) \\
P_e - Z_c U_e = \frac{\beta_0}{1 - \alpha_1 z^{-1}} z^{-D}(P_s - Z_c U_s)
\end{cases}
$$
(17)

where $\frac{b_0}{1 - a_1 z^{-1}} z^{-2D}$ is a first order digital filter modelling the propagation over a length $2L$. It replaces the filter $\left(\frac{\beta_0 z^{-D}}{1 - \alpha_1 z^{-1}} \right)^2$ appearing in equation (7) modelling the propagation over a length $2L$ as the product of two filters corresponding to the propagation over a length L.

In order to remove the variables p_s and u_s delayed of $(D + 1)$ in the first equation of system (17), we assume $\alpha_1 = a_1$. This means that the rate of frequency variations of the losses are assumed to be similar for the propagation over a length L (determined by the value of α_1) and over a length $2L$ (determined by the value of a_1). By counterpart, the coefficient β_0 is changed into a coefficient β_{0ap} in order to keep the height of the first impedance peak the frequency of which is $\frac{c}{4L}$, which requires:

$$
\left| \frac{\beta_{0ap}}{1 - a_1 \tilde{z}^{-1}} \right|^2 = \left| \frac{b_0}{1 - a_1 \tilde{z}^{-1}} \right|
$$
(18)

where $\tilde{z} = e^{j\tilde{\omega}}$ and $\tilde{\omega} = \frac{\pi c}{2L}$, which yields:

$$
\beta_{0ap} = \sqrt{b_0 \sqrt{1 - 2a_1 cos(\tilde{\omega}) + a_1^2}}
$$
(19)

With these modifications and dimensionless variables, the system of equations (17) becomes:

$$
\begin{cases}
b_0(\tilde{p}_e(n - 2D) + \tilde{u}_e(n - 2D)) = \\
\quad \beta_{0ap}(\tilde{p}_s(n - D) + \tilde{u}_s(n - D)) \\
\tilde{p}_e(n) = \tilde{u}_e(n) + a_1(\tilde{p}_e(n - 1) - \tilde{u}_e(n - 1)) \\
\quad + \beta_{0ap}(\tilde{p}_s(n - D) - \tilde{u}_s(n - D))
\end{cases}
$$
(20)

Using the same calculation as the one of the previous subsection, the first equation of system (20) provides analytically the value of $\tilde{u}_s(n - D)$:

$$
\tilde{u}_s(n - D) = \text{sign}(\tilde{V}_s) \frac{-\beta_{0ap} + \sqrt{\beta_{0ap}^2 + 4 \text{ sign}(\tilde{V}_s) \beta_{0ap} \tilde{\alpha} \tilde{V}_s}}{2\beta_{0ap} \tilde{\alpha}}
$$
(21)

where $\tilde{V}_s$ is defined by:

$$
\tilde{V}_s = b_0(\tilde{p}_e(n - 2D) + \tilde{u}_e(n - 2D))
$$
(22)

As a second approximation, the nonlinear losses coefficient $\tilde{\alpha}$ is assumed to remain small. This allows a second order series expansion of equation (21) which leads to:

$$
\tilde{u}_s(n - D) \simeq \frac{\tilde{V}_s}{\beta_{0ap}} - \tilde{\alpha} \text{ sign}(\tilde{V}_s) \frac{\tilde{V}_s^2}{\beta_{0ap}^2}
$$
(23)

This finally yields the following computation scheme expressing $\tilde{p}_e(n)$ with respect to $\tilde{u}_e(n)$, $\tilde{p}_e(n - 2D)$ and $\tilde{u}_e(n - 2D)$:

$$
\begin{cases}
\tilde{V}_s = b_0(\tilde{p}_e(n - 2D) + \tilde{u}_e(n - 2D)) \\
\tilde{V} = a_1[\tilde{p}_e(n - 1) - \tilde{u}_e(n - 1)] \\
\quad - \tilde{V}_s + 2 \text{ sign}(\tilde{V}_s) \frac{\tilde{\alpha}}{\beta_{0ap}} \tilde{V}_s^2 \\
\tilde{p}_e(n) = \tilde{u}_e(n) + \tilde{V}
\end{cases}
$$
(24)

2.4. Role of the nonlinear termination on the bore response

In order to study the role played by the nonlinear termination, we consider a transient flow excitation of the form: $\tilde{u}_e(t) = \lambda \delta(t)$ and computes with the most accurate nonlinear model $\tilde{p}_e(n)$ for several values of λ, as well as the ratio of the Fourier transforms of $\tilde{p}_e$ and $\tilde{u}_e$. For these examples, the output radius r_t is assumed to be smaller than the bore input radius R: $r_t = \frac{R}{3}$.

Figures (1) and (2) show respectively the first two reflections of the impulse response and the ratio of the Fourier transforms of the dimensionless pressure and flow: $Z_{eq}(\omega) = \frac{\tilde{P}_e(\omega)}{\tilde{U}_e(\omega)}$ in the linear case and in the nonlinear case, with $\lambda = 10^{-5}$. With such a small value of λ, the effects of the nonlinear termination are not significant, and $Z_{eq}(\omega)$ corresponds to the input impedance of the bore (linear case).
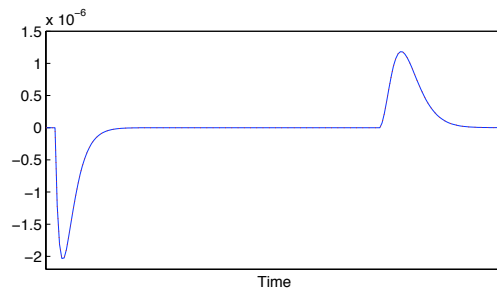

Figure 1: *First two reflections of the impulse response. $\lambda = 10^{-5}$. Solid line : nonlinear case. Dotted line: linear case. Nonlinear and linear cases are exactly superimposed.*

Figures (3) and (4) show the same computations for $\lambda = 0.5$. The effects of the nonlinear termination are clearly visible. In particular, the damping of the first reflection is much more important than in the linear case and the peaks of $Z_{eq}(\omega)$ are smaller than in the linear case. It is worth noting that opposite to the case of linear losses (taken into account by a radiation impedance) that become significant at high frequencies, the nonlinear losses are significant at low frequencies. This suggests that, depending on the flow level in the mouthpiece, the nonlinear termination may modify the functioning of the whole instrument.
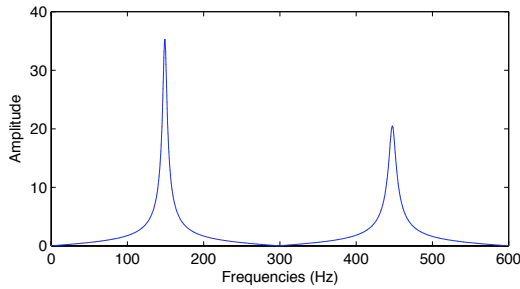
Figure 2: *Fourier transform of the response to a Dirac excitation.* $\lambda = 10^{-5}$. *Solid line : nonlinear case. Dotted line: linear case. Nonlinear and linear cases are exactly superimposed.*
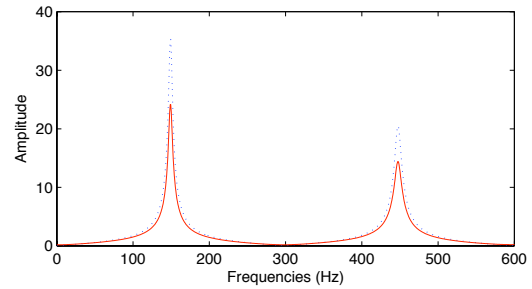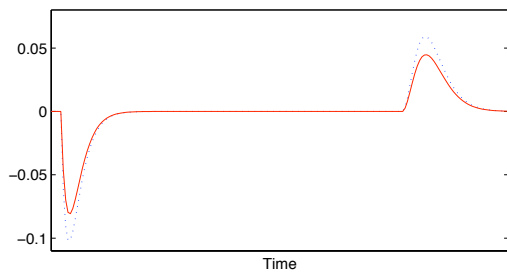

Figure 3: *First two reflections of the impulse response.* $\lambda = 0.5$. *Solid line : nonlinear case. Dotted line: linear case.*

3. FULL INSTRUMENT MODEL

In this section, the modifications of the functioning of the instrument induced by the presence of the nonlinear termination are studied. For that purpose, we first recall the classical physical model of the nonlinear coupling between the reed and the bore.

3.1. Physical model

The physical model describes first the dimensionless displacement $x(t)$ of the reed with respect to its equilibrium point by:

$$\frac{1}{\omega_r^2}\frac{d^2 x(t)}{dt^2} + \frac{q_r}{\omega_r}\frac{dx(t)}{dt} + x(t) = \tilde{p}_e(t) \qquad (25)$$

where $\omega_r = 2\pi f_r$ and q_r^{-1} are respectively the circular frequency and the quality factor of the reed.

The opening of the reed channel $S_r(t)$ is expressed from the reed displacement by:

$$S_r(t) = \Theta(1 - \gamma + x(t)) \times \zeta(1 - \gamma + x(t))$$

where Θ denotes the Heaviside function. Its role is to keep the opening of the reed channel positive by cancelling it when $1 - \gamma + x(t) < 0$. The parameter ζ characterizes the whole embouchure and is proportional to the square root of the reed position at equilibrium H. The dimensionless parameter γ is the ratio between the blowing pressure p_m and the static beating reed pressure p_M defined by: $p_M = \mu_r H \omega_r^2$, where μ_r is the mass per unit-surface of the reed.

Figure 4: *Fourier transform of the response to a Dirac excitation.* $\lambda = 0.5$. *Solid line : nonlinear case. Dotted line: linear case.*

The nonlinear characteristics is based on the stationary Bernoulli equation and links the acoustic flow (the product between the opening of the reed channel and the acoustic velocity) to the pressure difference between the bore and the mouth of the player. It is given by:

$$\tilde{u}_e(t) = S_r(t)\text{sign}(\gamma - \tilde{p}_e(t))\sqrt{|\gamma - \tilde{p}_e(t)|} \qquad (26)$$

These equations are discretized according to the schemes presented in [6]. The third part of the full digital model is made of the bore, the two digital models of which have been presented in the previous section. The way the nonlinear bore models have been written makes their use straightforward in our synthesis scheme. The external pressure is computed by the time derivative of the output flow $\tilde{u}_s(t)$.

3.2. Results

In this part, both the role of the nonlinear termination and the relevance of the simplified nonlinear bore model are studied.

In the following examples, the output radius r_t is: $r_t = \frac{R}{2}$. The value of the parameter ζ is: $\zeta = 0.34$. The reed resonance frequency is $2200 Hz$ and the reed quality factor is 0.4. According to the values of the physical parameters, the weight $\tilde{\alpha}$ of the nonlinear termination is: $\tilde{\alpha} = 0.113$.

3.2.1. Steady-state oscillations

Figure 5 shows one period of the steady state oscillations of the pressure (top) and the flow (bottom) of a sound generated with a constant value of $\gamma = 0.42$. Though the blowing pressure is small, the effect of the nonlinear termination appears clearly.

Figure 6 shows the ratio of the Fourier transforms of the pressure and flow in the mouthpiece corresponding to $\gamma = 0.42$. The linear case, displayed in dotted line, corresponds to the input impedance of the bore. The nonlinear cases, displayed in solid line and dashed line, exhibit a strong lowering of the first peak (about two times smaller) and a smaller lowering of the second peak. Again, though the blowing pressure is small, the effect of the nonlinearity is clearly visible.

Both in the time and frequency domains, the difference between the accurate nonlinear model and the approximated nonlinear model is very small.

Figure 7 shows one period of the steady state oscillations of the pressure (top) and the flow (bottom) of a sound generated with a constant value of $\gamma = 0.56$. For this blowing pressure which is above the beating-reed pressure corresponding to $\gamma = 0.5$, the
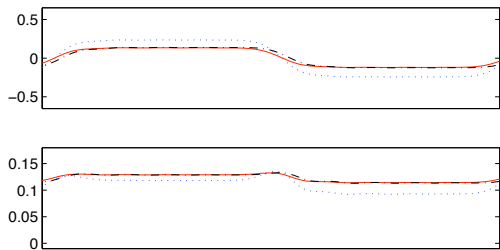
Figure 5: *Top: mouthpiece pressure. Bottom: mouthpiece flow (γ = 0.42). Dotted line : linear case. Solid line : accurate model. Dashed line: approximated model.*

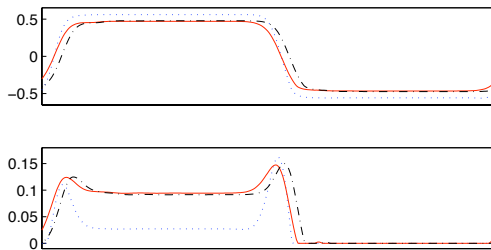Figure 7: *Top: mouthpiece pressure. Bottom: mouthpiece flow (γ = 0.56). Dotted line : linear case. Solid line : accurate model. Dashed line: approximated model.*
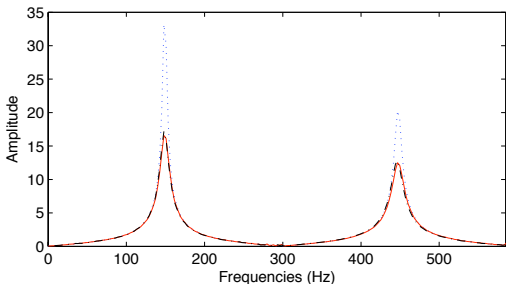

Figure 6: *Ratio of the Fourier transforms of the mouthpiece pressure and flow (γ = 0.42). Dotted line : linear case. Solid line : accurate model. Dashed line: approximated model.*
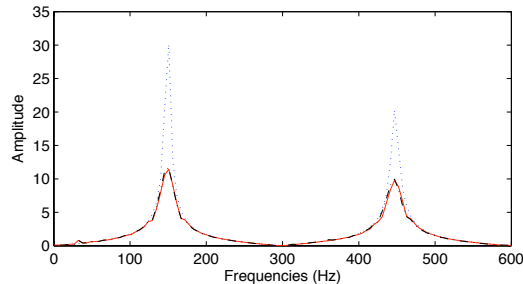

Figure 8: *Ratio of the Fourier transforms of the mouthpiece pressure and flow (γ = 0.56). Dotted line : linear case. Solid line : accurate model. Dashed line: approximated model.*

effects of the nonlinear termination produce an important modification of the acoustic flow.

Figure 8 shows the ratio of the Fourier transforms of the pressure and flow in the mouthpiece corresponding to $\gamma = 0.56$. Compared to the linear case (dotted line), the nonlinear cases (solid line and dashed line) exhibit a drastic lowering of the first peak (about three times smaller) and an important lowering of the second peak. For such a blowing pressure, the effect of the nonlinearity is very important.

As it was the case for a smaller blowing pressure, the difference between the accurate nonlinear model and the approximated nonlinear model is not noticeable, showing that for synthesis purposes, the second order series expansion of the flow proposed in equation (23) is sufficient.

3.2.2. Increasing blowing pressure

In this example, the sound duration is $1.5s$. On this duration, the dimensionless blowing pressure γ increases linearly from 0.4 (around the self-oscillation threshold) to 0.95 (around the complete closure of the reed channel and stop of the self-oscillations).

Figure 9 compares the envelopes of the external pressure in the linear (left) case and the nonlinear (right) case. The nonlinear case is computed with the most accurate algorithm. The average sound level is smaller in the nonlinear case than in the linear case. While the sound level is continuously increasing in the linear case, one can observe that after an increasing phase, it decreases in the nonlinear case. Indeed, the synthesis shows that the output flow reaches a saturation level while the external pressure, correspond-

ing to the time derivative of the output flow, exhibits a decreasing spectral richness.
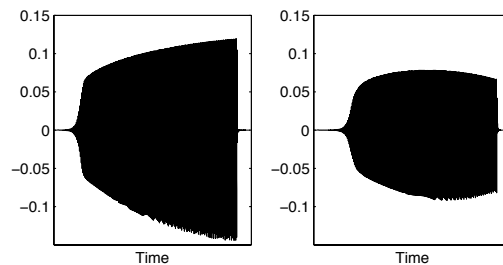

Figure 9: *External pressures corresponding to a linear increase of the blowing pressure. Left: linear case. Right: nonlinear case with accurate model.*

Pictures 10 and 11 show respectively the spectrogram of the external pressure in the linear case and in the nonlinear case. The vertical axis is frequency, from 0 to $4kHz$ and the horizontal axis is time, in seconds. It can be noticed that the birth of the fundamental frequency happens at the same time on both pictures. In the nonlinear case, the raising of the harmonics occurs later than in the linear case. The behavior of the even harmonics (coming from the mouthpiece flow, since the mouthpiece pressure contains very few even harmonics due to the impedance relationship) is significantly different: for small values of γ, the level of the amplitudes of the

even harmonics compared to that of the odd harmonics is higher in the nonlinear case than in the linear case. While the low order even harmonics keep a nearly constant level on the whole duration of the sound in the linear case, they first increase, then decrease until a minimum and increase again in the non linear case. It can be noticed that the time for which the even harmonics are minimum depends on their ranks; harmonic 2 has its minimum around $t = 1.1s$ while harmonic 12 has its minimum around $t = 0.8s$.

We point out that "usual" playing conditions correspond to the first $0.5s$ of the sound and that from a perceptual point of view, the most noticeable difference between the linear and nonlinear case is the balance between odd and even harmonics.
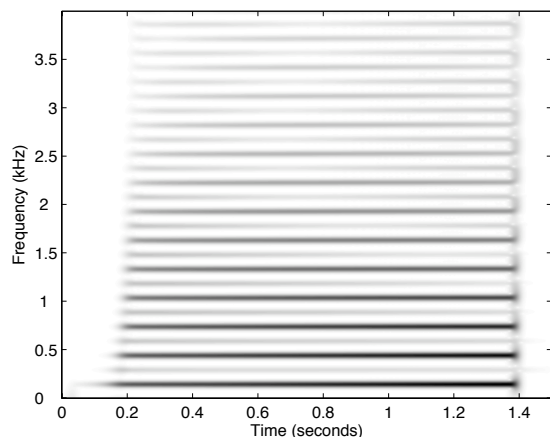

Figure 10: *Spectrogram of the external pressure corresponding to the linear case and a linear increase of the blowing pressure.*
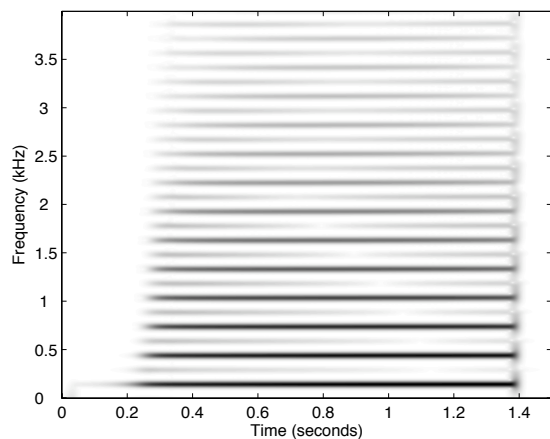

Figure 11: *Spectrogram of the external pressure corresponding to the nonlinear case and a linear increase of the blowing pressure.*

4. CONCLUSION

Confirming the results of Atig [2] and extending them to the case of frequency dependant bore losses and reed with mass, it has been shown that the introduction of nonlinear losses modifies significantly the role of the bore at low frequencies, hence affecting the functioning and the timbre of the instrument.

The work presented in this paper constitutes a first step towards a simple, dynamic nonlinear tonehole model extending the results presented in [9]. Moreover, during attacks consisting in a sudden burst of the blowing pressure, the effect of the nonlinear termination may modify the features of the transient.

Despite its simplicity and low computation cost, the simplified nonlinear model provides results fully similar to those of the more accurate model and seems applicable to the case of more complex bore geometries since it only adds to the resonator model a nonlinear function of the time-delayed variables at the mouthpiece level thanks to the removal of the variables at the open end level.

Sound examples are available at:
http://www.lma.cnrs-mrs.fr/~guillemain/DAFX06/dafx06.htm

5. REFERENCES

[1] V. Dubos, J. Kergomard, A. Khettabi, J. Dalmont, D. Keefe, and C. Nederveen, "Theory of sound propagation in a duct with a branched tube using modal decomposition," *Acustica - Acta Acustica*, vol. 85, pp. 153–169, 1999.

[2] M. Atig, "Non-linéarité acoustique localisée à l'extrémité ouverte d'un tube. mesure, modélisation et application aux instruments à vent," Ph.D. dissertation, Université du Maine, 2004.

[3] G. Scavone and P. Cook, "Real-time computer modeling of woodwind instruments," in *Proc. ISMA 1998*, Leavenworth, WA, USA, 1998.

[4] M. van Walstijn and G. Scavone, "The wave digital tonehole model," in *Proc. Int. Comp. Music Conf. (ICMC'00),* Berlin, Germany, 2000.

[5] J. Dalmont, C. Nederveen, V. Dubos, S. Ollivier, V. Méserette, and E. te Sligte, "Experimental determination of the equivalent circuit of an open side hole: linear and non linear behaviour," *Acustica - Acta Acustica*, vol. 88, pp. 567–575, 2002.

[6] P. Guillemain, J. Kergomard, and T. Voinier, "Real-time synthesis of clarinet-like instruments using digital impedance models," *J. Acoust. Soc. Am.*, vol. 118, no. 1, pp. 483–494, 2005.

[7] A. Pierce, *Acoustics.* NY: McGraw-Hill, 1981.

[8] T. A. Wilson and G. S. Beavers, "Operating modes of the clarinet," *J. Acoust. Soc. Am*, vol. 56, pp. 653–658, 1974.

[9] J. Terroir and P. Guillemain, "A simple dynamic tone hole model for real-time synthesis of clarinet-like instruments," in *Proc. Int. Comp. Music Conf. (ICMC'05),* Barcelona, Spain, 2005.